A Tomographic Image of Western United States Late-stage Orogeny

Brandon Schmandt[1] & Eugene Humphreys[1]

[1]*Department of Geological Sciences, University of Oregon, Eugene, Oregon 97403, USA*

Seismic study of upper mantle structure has brought a progressive growth in recognition of the large magnitude and wide range in scale length of structure beneath continents, and a similar growth in understanding of the importance of sub-lithospheric processes on tectonic and magmatic activity. Using distant earthquakes recorded by the EarthScope Transportable Array and more than 1500 additional stations, we present the first high-resolution P-wave, S-wave and V_P/V_S tomographic images of the entire western United States upper mantle. We then use information on western United States tectonic and volcanic activity to account for the creation one of Earth's great orogenic plateaus, a process that we attribute largely to the Laramide-age emplacement of a flat-subducting slab beneath most of the western United States and its subsequent (and continuing) removal. This orogeny has created strong compositional, structural and thermal heterogeneity in the western United States crust, lithosphere and underlying convecting mantle.

The western U.S. provides an excellent region for advancing our understanding of mantle heterogeneity caused by subduction, small-scale convection of the lithosphere, and plumes[1-4]. Seismologists have long recognized that subduction beneath western U.S. occurs into an upper mantle that is anomalously slow[5,6]; on average, mantle seismic velocities between 100-200 km depth are among Earth's slowest[6,7]. Imaged within this generally slow mantle are small-scale high-velocity structures that exhibit seismic contrasts as great as that observed between average craton and the western U.S.[8] That the western U.S. upper mantle is vigorously active is implicated by geologic study, which has shown that the western third of the U.S. is undergoing post-Laramide orogenic collapse[9,10] with accompanying volcanism, and it has been uplifted into one of Earth's great plateaus. The elevated western U.S. interior is comprised of distinctive tectonic and geomorphic provinces, including the highly extended and magmatically altered Basin and Range, the Laramide-contracted and unextended Colorado Plateau and Rocky Mountains, and the tilted and intact Great Plains. It appears that large portions of the Great Plains, Rocky Mountains and Colorado Plateau have been uplifted in part since the Laramide orogeny[11], with evidence for uplift continuing to the present[12,13]. This indicates young and ongoing mass redistribution at depth.

Ongoing transition of the westernmost North America margin from subduction to transform[14] has been used to predict a triangular slab-free area beneath most of the Basin and Range and southern Rocky Mountains[15], although the geologic evidence for complex subduction during the past 75 Ma suggests that the actual slab distribution may be more complicated. In particular, the distribution of Laramide thrust faulting and magmatism suggests flat-slab subduction as far east as the Rocky Mountain Front[16], and the subsequent ignimbrite flareup of the Basin and Range is thought to represent slab removal[17] beneath the Basin and Range[18]. Accretion of the Siletzia ocean lithosphere ~50 Ma necessitated abandonment of the Challis subduction zone, slab tearing, and initiation of subduction at Cascadia[19-21]. The fate and distribution of ~5000 km of slab subducted 75-20 Ma has been the subject of recent seismic investigations[1,22-24].

Seismic Results

In this paper we present new tomography models for P and S velocity (V_P and V_S) of the western U.S. mantle to depths of 800 km. Our use of nearly all available data results in upper mantle resolution superior to previous efforts, and our imaging of V_P/V_S structure help identify where properties other than temperature have a strong influence on imaged velocity perturbations.

Our data are teleseismic travel-time residuals, which we invert for 3-D V_P, V_S and V_P/V_S perturbations using frequency-dependent 3-D sensitivity kernels[25]. Data from 850 EarthScope transportable array (TA) stations are combined with data from 25 permanent and temporary networks for total of 2,500 stations and 230,000 P-wave arrivals, and 1,300 stations and 80,000 S-wave arrivals (Fig. 1). Residual times for the TA and all concurrently operating stations are measured in overlapping regional sub-arrays, each with approximately eight degrees aperture. Sub-array dimensions are selected to coordinate with the movement of the TA and optimize waveform coherency and use of high-quality teleseismic events. Residual times are measured by cross-correlation of band-pass-filtered waveforms in up to four narrow-frequency bands. We use recent advances in western U.S. crust thickness[26] and velocity[27] models to better isolate the mantle component of residual times. More details on data analysis, inversion technique, model resolution and the complete tomographic models are given in the Supplementary Information.

In general, strong multi-scale heterogeneity exists throughout the western U.S. upper mantle. The most striking aspect of our images is the prominence of strong V_P and V_S structure in the upper 250 km over a range of length scales. Amplitudes diminish with depth, although major high-velocity structures thought to represent relict subducted slab are found across the upper mantle and transition zone. V_P and V_S models are highly mutually consistent, and slow volumes generally have elevated V_P/V_S. Physical origins of seismic velocity variations are variations in temperature, partial melt, anisotropy, bulk and volatile composition. Seismic structure of magnitude as great those imaged, however, must include an important contribution from temperature. Hence, the imaged structure must be young and transient in nature and represent convection (including subduction) occurring on multiple spatial and temporal scales. Because most of the strong small-scale features lie within or below the region occupied by the flat-subducting Farallon slab during the Laramide orogeny, these structures were created during or after the Laramide.

Strong V_P/V_S variations above ~200 km and weak temperature dependence of V_P/V_S in solid-state peridotite[28] lead us to infer that partial melt and dissolved volatiles[29] contribute significantly to low-velocity, high V_P/V_S upper mantle, with volatiles required below ~70 km and partial melt expected in the lowest-velocity and highest V_P/V_S mantle (further discussion in the Supplementary Information). Because the volumes of highest V_P/V_S are in the shallow mantle beneath areas of young magmatism, partial melt is the obvious explanation for large velocity reductions with respect to the already slow mean. We expect that varying degrees of melt depletion[28], and simply the absence of partial melt, account for most of the low to neutral V_P/V_S regions in the shallow upper mantle. Near vertical alignment of olivine a-axes, owing to vertical strain in convective downwellings[30] or down-dip anisotropy in steeply subducting slabs, may also contribute to low Vp/Vs in such high-velocity features.

Tectono-magmatic Interpretation

The breadth and detail of new tomographic models allow us to draw reasoned conclusions about the geologic origin of western U.S. upper mantle structure by considering imaged features in the context of western U.S. tectono-magmatic history. The imaged mantle structure also affords us the opportunity to provide an improved accounting for the Cenozoic evolution of western U.S. into one of Earth's great orogenic plateaus.

Beneath most of Wyoming, northeast Utah, and northwest Colorado, high-velocity mantle extends to depths of 250-300 km (Fig. 2). It is difficult to explain how the ~2 km uplift of this area from near sea level at times prior to the Laramide orogeny can be made consistent with a lithosphere thickness as great or greater than that typically found beneath cratons[6,7]. We propose that a buoyant ocean plateau inferred to have subducted during the Laramide orogeny (the Shatsky rise conjugate) stalled beneath this region. Subduction of the plateau beneath North America is thought to have caused slab flattening, erosion of basal lithosphere[31], and movement of the Colorado Plateau northeast into North America, creating the Laramide basement-cored uplifts of the Rocky

Mountains. The time and location of plateau subduction is best resolved by the geologic record of its impact at ~85 Ma near southern California. Following Saleeby[32-34], we assume the ocean plateau moved approximately to the northeast within a non-deforming subducted Farallon plate as far inboard as Wyoming and South Dakota. Transfer of the plateau lithosphere from the subducted Farallon to basal North America lithosphere is compatible with the imaged bight in the deep Farallon beneath Hudson Bay[35], and the implied decrease in coupling between the subducting Farallon and North America is approximately concurrent with 60 Ma rapid motion of North America toward the subduction zone[36]. Wyoming elevation is attributed to replacement of the eroded base of North America with buoyant ocean-plateau lithosphere (Fig. 3b). The presence of lateral buoyancy variations in the Farallon slab offers a mechanical explanation for the dissected geometry of the inferred Laramide-age subducted slab and the chaotic distribution of volcanism thought to represent flat-slab emplacement and removal beneath the Rocky Mountains.

Most of the Colorado Plateau is distinguished from the surrounding Basin and Range and Rio Grande Rift provinces by laterally continuous high-velocity mantle from 60–125 km depth (Fig. 1, 2). However, at the same depths the margin of the Colorado Plateau, and especially the southwestern plateau (including the Grand Canyon and San Francisco Peaks volcanic field) is underlain by low-velocity mantle similar to that of the Basin and Range. In addition, isolated, high-velocity volumes extend beneath central-southern Utah and northwestern New Mexico[37] to depths of ~230 km and ~200 km, respectively (Fig. 2c). This mantle structure, in conjunction with the elevated plateau rim[13] and late-Cenozoic migration of volcanism onto the Colorado Plateau[38] suggests heating[38] and approximately concentric erosion[13] of a step in lithospheric thickness originally located beneath the topographic boundary. The presence of two deeper, drip-like high-velocity bodies and the absence of thick high-velocity mantle lithosphere beneath much of the southwestern Colorado Plateau indicates that more localized downwellings of either North America mantle lithosphere or Farallon lithosphere are also important to the Cenozoic evolution of the plateau. Given the near-boundary location of these structures, it appears that this convection may simply represent acceleration of edge-driven processes resulting from 3-D heterogeneity in the Colorado Plateau lithosphere. An episode of enhanced removal of lithospheric mantle is likely responsible for a 28–16 Ma pulse of unroofing on the southwestern Colorado Plateau[39].

A high-velocity "curtain" extends vertically from near the base of the lithosphere to depths of ~240 km beneath Washington and ~450 km beneath northern Idaho and western Montana (Fig. 2, 3c). Subducted slab is the only plausable origin for a volume of mantle this large and as fast than the Juan de Fuca slab (i.e., the near-vertical high-velocity structure imaged beneath the Cascades) (Fig. 3c). Because this curtain of fast mantle roughly follows the inferred Siletzia subduction zone on the north and east side of Siletzia, it most likely is Farallon slab that was attached to the leading margin of Siletzia when it accreted ~50 Ma. The Challis arc generally is thought to involve subduction although the variety of volcanic products suggests unusual subduction[19], such as subduction of a spreading center[20]. Assuming a subducted-slab origin for the high-velocity "curtain", the slab must be of near-neutral buoyancy to have neither sunk nor been swept away by larger-scale mantle flow for ~50 m.y. Plate-tectonic reconstructions have young (5–20 My) lithosphere subducting beneath the Pacific Northwest at this time[20,36], and hence initial slab buoyancy would have been nearly neutral, with modest negative thermal buoyancy balanced by a positive compositional buoyancy created by basalt depletion during ocean-lithosphere creation[40]. Without a large temperature anomaly, the 2-3% V_P anomaly is primarily attributed to the effects of basalt depletion and accompanying ocean lithosphere dehydration, which would contrast with the generally hydrated or partially molten western U.S. asthenosphere.

Several high-velocity structures in the depth range ~100-200 km reside adjacent to unusually low-velocity, high V_P/V_S mantle (Fig. 2c). We infer that these low-velocity volumes are ascending and melting return flow driven by nearby negatively buoyant downwellings imaged as high-velocity bodies. Because the maintenance of significant melt fraction is transient, we think that the paired volumes of fast and very slow, high V_P/V_S mantle represent the most active convective systems imaged. The occurrence of vigorous small-scale convection accompanied by partial melting is supported by young uplift and magmatism above these paired short-wavelength and high-amplitude mantle velocity anomalies. Small-scale upper mantle convection involving the recent sinking of dense mafic roots created by deep crustal segregation of granite plutons has been proposed for the uplifted southern Sierra Nevada[3] and Wallowa Mountains[41]. Similar decompression-induced partial melting is thought to create very slow mantle near the southern edge of the Gorda-Juan de Fuca slab, where toroidal flow of oceanic asthenosphere around the slab is expected to have an upward poloidal component[42], and beneath the Salton Trough, where plate spreading at the northernmost East Pacific Rise drives mantle ascent (Fig 2a).

The most prominent low-velocity, high V_P/V_S upper mantle volume occupies the ~200 km beneath Yellowstone and the eastern Snake River Plain (Fig. 2, 4). A broader low-velocity volume occupies the transition zone beneath the Yellowstone region. It appears separate from the shallow anomaly in the P-wave model and perhaps weakly connected in the S-wave model. A ~12 m geoid high centered on Yellowstone indicates that the high Yellowstone topography is compensated at depths greater than the rest of elevated western U.S., which is attributed to the buoyancy of the very low velocity mantle imaged in the upper ~200 km beneath Yellowstone[43,44,4]. The prominence of shallow and deep low-velocity mantle below the Yellowstone region suggests a supply from a zone of unusually hot or chemically heterogeneous mantle within the transition zone. Recent modeling of seismic multi-pathing suggests a thin (~50 km) conduit may connect the shallow and deep anomalies[45], and it is likely that wave-front healing and regularization would cause such a structure to be obscured in our travel-time imaging. The proximity of major high-velocity bodies suggests that ascending mantle beneath Yellowstone is driven by sinking cool masses as well as its own positive buoyancy (Fig. 2). Yellowstone's highly organized surface expression[46] appears to be as much a consequence of plume interactions with the lithosphere as with a stable, deep source.

A volumetrically large, strongly anomalous high-velocity body imaged in the transition zone beneath central Nevada to eastern Colorado and Wyoming (Figs. tomo and X) must be subducted ocean lithosphere. Paleo-trench modeling[47] predicts the ~30–55 Ma subducted lithosphere at this horizontal location. However, it remains a challenge to determine how the large volume of dismembered high-velocity structures relates to the ~6500 km of ocean lithosphere that has subducted since the Laramide orogeny began[34,35].

Discussion

Our imaging provides new insight into the causes and consequences of western U.S. tectonism and magmatism. The thick, high-velocity and buoyant structure beneath Wyoming is attributed to the accretion of an oceanic plateau onto the base of North America. We have insufficient information to understand either the mechanism of transfer to North America or quantify the lithosphereic density structure. However, this accreted ocean lithosphere must contribute to isostatic support of approximately 2 km of post-Cretaceous uplift and it appears to be a stable addition to the continental lithosphere. In contrast, the high-velocity curtain of presumed slab abandoned beneath the Pacific Northwest is nearly neutrally buoyant and it probably will be swept away at some time in the future. However, the accretion of Siletzia to the margin of North America represents real continental growth, and the low elevation and mechanical strength of this lithosphere can be attributed to its oceanic origin[21]. The westward jump in subduction to Cascadia associated with Siletzia accretion must have torn the subducting Farallon slab beneath central Oregon. It is at this time and place that the vigorous ignimbrite flareup began[48], with progressive removal of the flat slab initiating advective heating and melt depletion of the Laramide-affected lithosphere[49].

Conclusion

Tectonism and magmatism distributed across western U.S. has created small-scale heterogeneities that are organized into regional provinces that together comprise the elevated western U.S. Most of this activity was driven and organized by a relatively simple event – the insertion and removal of flat-subducting slab beneath the provincially heterogeneous western U.S. Uplift of the flat-slab affected area involves the disruption of a stable continental lithosphere by a diverse set of uppermost mantle buoyancy contributions: erosion of basal North America thermal lithosphere; lithospheric heating (mostly through melt ascent); depletion of mantle lithosphere through melt extraction; and the emplacement of depleted ocean lithosphere. This heterogeneity was partly controlled by pre-existing lithospheric heterogeneity, as evidenced by geologic provinces, and the more recently acquired heterogeneity represents modification of these ancient geologic provinces. A further result of slab flattening and removal has been the creation of a heterogeneous sub-lithospheric mantle that is littered with fragments of Laramide and post-Laramide subducted slab and delaminated bits of North America lithosphere. The imaged structure is the clutter left behind by a major continental reconstruction event, and on the limited space and time scales that we have considered, the overall effect of this event on the mantle has been a net creation of heterogeneity.

1. Sigloch, K., McQuarrie, N., & Nolet, G. Two-stage subduction history under North America inferred from multiple-frequency tomography, *Nature Geoscience*, **1**, 458–462 (2008).

2. Bird, P., Continental delamination and the Colorado Plateau, *J. Geophys. Res.*, **84**, 7561–7571 (1979).

3. Zandt, G., et al., Active foundering of a continental arc root beneath the southern Sierra Nevada in California, *Nature*, **431**, 41–46 (2004).

4. Schutt, D. L., Dueker, K., Temperature of the plume layer beneath the Yellowstone hotspot, Geology, **36**, no. 8, 623–626, doi: 10.1130/G24809A (2008).

5. Romanowicz, B., Seismic structure of the upper mantle beneath the United States by three dimensional inversion of body wave arrival times, *Geophys. J. R. astr. Soc.*, **57**, 479–506 (1979).

6. Grand, S. P., Mantle shear structure beneath the Americas and surrounding oceans, *J. Geophys. Res*., **99**, 11,591–11,621 (1994).

7. Lebedev, S. & van der Hilst, R., Global upper mantle tomography with the automated inversion of surface and S-waveforms, Geophys. J. Int., **173**, 505-518 doi: 10.1111/j.1365-246X.2008.03721.x (2008).

8. Humphreys, E. and Dueker, K. (1994). Western US upper mantle structure,

J. Geophys. Res., **99**, 9615–9634.

9. Burchfiel, B. C., Cowen, D. S., & Davis, G. A., (1992), in *The Geology of North America: The Cordilleran Orogen: Conterminous U.S.* (eds Burchfiel, B. C., Lipman, P., & Zoback, M. L.) **G-3**, 407–479, (Geological Society of America, Boulder, Cololorado, 1992).

10. Coney, P. J., & Harms, T. A., Cordilleran metamorphic core complexes: Cenozoic

extensional relics of Mesozoic compression, *Geology*, **12**, 550–554 (1984).

11. Heller, P. L., K. Dueker, M. McMillan, Post-Paleozoic alluvial gravel transport as evidence of continental tilting in the Cordilleran, United States, *Geol. Soc. Am. Bull*., **115**, 1122–1132 (2003).

12. Riihimaki, C. A., R. S. Anderson, E. B. Safran, Impact of rock uplift on rates of late Cenozoic Rocky Mountain river incision, J. Geophys. Res., **112**, F03S02, doi:10.1029/2006JF000557 (2007).

13. Karlstrom, K. E, Crow, R., Crossey, L. J., Coblentz, D. & Van Wijk, J. W., Model for tectonically driven incision of the younger than 6 Ma Grand Canyon, *Geology*, **36**, 835–838, doi: 10.1130/G25032A.1 (2008).

14. Atwater, T., Implications of plate tectonics for Cenozoic tectonic evolution of western North America, *Geol. Soc. Am. Bull*., **81**, 3513–3536 (1970).

15. Dickinson, W.R., & Snyder, W.S., Geometry of subducted slabs related to the San Andreas transform, *J. Geology*, **87**, 609–627 (1979).

16. Bird, P., Laramide crustal thickening event in the rocky mountain foreland and great plains, *Tectonics*, **3**, 741–758 (1984).

17. Coney, P. J., & S. J. Reynolds, Flattening of the Farallon slab, *Nature*, **270**, 403–406 (1977).

18. Humphreys, E. D., Post-Laramide removal of the Farallon slab, western United States, *Geology*, **23**, 987–990 (1995).

19. Christiansen, R. L., & Yeats, R. S., in *The Geology of North America: The Cordilleran Orogen: Conterminous U.S.* (eds Burchfiel, B. C., Lipman, P., & Zoback, M. L.) **G-3**, 261–406, (Geological Society of America, Boulder, Cololorado, 1992).

20. Madsen, J.K., Thorkelson, D. J., Friedman, R. M., & Marshall, D. D., Cenozoic to

Recent plate configurations in the Pacific Basin: Ridge subduction and slab window magmatism in western North America, *Geosphere*, 2, 11–34 (2006).

21. Humphreys, E., in *Circum-Pacific Tectonics, Geologic Evolution, and Ore Deposits* Cenozoic (eds. Spencer, J. E., & Titley S.), 389–396 (Arizona Geological Society Digest 22, 2009).

22. Van der Lee, S., & Nolet, G., Seismic image of the subducted trailing fragments of the Farallon plate, Nature 386, 266 - 269 (1997).

23. Burdick, S., et al., Model Update December 2008: Upper Mantle Heterogeneity beneath North America from P-wave Travel Time Tomography with Global and USArray Transportable Array Data, Seis. Res. Lett. **80**(4), 638 – 645 (2009).

24. Roth, J. B., Fouch, M. J., James, D. E., & Carlson, R. W., Three-dimensional seismic velocity structure of the northwestern United States, *Geophys. Res. Lett.* **35**, L15304 (2008).

25. Dahlen, F.A., Hung, S.-H., Nolet, G. (2000) Frechet kernels for finite-frequency traveltimes, I. Theory, *Geophys. J. Int.*, **141**, 157–174 (2000).

26. Lowry, A. R., Squeezing Mass Structure from EarthScope TA Data, EarthScope National Meeting abstract, (2009).

27. Lin, F-C., Moschetti, M. P., Ritzwoller, M. H., Surface wave tomography of the western United States from ambient seismic noise: Rayleigh and Love wave phase velocity maps, Geophys. J. Int. **173**, 281–298 doi: 10.1111/j.1365-246X.2008.03720.x (2008).

28. Lee, C.-T. A., Compositional variation of density and seismic velocities in natural peridotites at STP conditions: Implications for seismic imaging of compositional

heterogeneities in the upper mantle, J. Geophys. Res., **108**(B9), 2441, doi:10.1029/2003JB002413, (2003).

29. Karato S., Jung H., Water, partial melting and the origin of seismic low velocity and high attenuation zone in the upper mantle. Earth Planet Sci Lett., **57**, 193-207 (1998).

30. West, J. D., Fouch, M.J., Roth, J.B., Elkins-Tanton, L.T., Vertical mantle flow associated with a lithospheric drip beneath the Great Basin, Nature Geoscience, **2**, 439-444 (2009).

31. Spencer, J. E., Uplift of the Colorado Plateau due to lithosphere attenuation during Laramide low-angle subduction, J. Geophys. Res., **101**, 13,595 – 13,609 (1996).

32. Saleeby, J., Segmentation of the Laramide Slab - evidence from the southern Sierra Neveda region, *Bull. Geol. Soc. Am*., **115**, 655–668 (2003).

33. Stock, J., & Molnar, P., Uncertainties and implications of the Late Cretaceous and Tertiary position of North America relative to the Farallon, Kula, and Pacific plates, *Tectonics*, **7**, 1339–1384 (1988).

34. Engebretsen, D. C., Cox, A., Gordon, R. G., Relative motions between oceanic and continental plates in the Pacific Basin, *Geol. Soc. Am.* (Spec. Pap.) **206**, 560–569 (1985).

35. Bunge, H.-P. & Grand, S. Mesozoic plate-motion history below the northeast Pacific Ocean from seismic images of the subducted Farallon slab. Nature **405**, 337–340 (2000).

36. Muller, R. D., Sdrolias, M., Gaina, G., & Roest, W. R, Age, spreading rates, and spreading asymmetry of the world's ocean crust, *Geochem. Geophys. Geosys.*, **9**, Q04006, doi:10.1029/2007GC001743 (2008).

37. Sine, C. R. et al. Mantle structure beneath the western edge of the Colorado Plateau. Geophys. Res. Lett. 35, doi:10.1029/2008GL033391 (2008).

38. Roy, M., Jordan, T. H., Pederson, J., Colorado Plateau magmatism and uplift by

warming of heterogeneous lithosphere, Nature, **459**, 978-982 (2009).

39. Flowers, R.M., Wernicke, B. P., Farley, K. A., Unroofing, incision, and uplift history of the southwestern Colorado Plateau from apatite (U-Th)/He thermochronometry, *Geol. Soc. Am., Bull.*, **120**, 571–587; doi: 10.1130/B26231.1 (2008).

40. Burkett, E. & Billen, M. I., Dynamics and Implications of Slab Detachment Due to Ridge-Trench Interaction, *J. Geophys. Res*., in review (2009).

41. Hales, T. C., Abt, D. L., Humphreys, E. D., Roering, J. J., A lithospheric instability origin for Columbia River flood basalts and Wallowa Mountains uplift in northeast Oregon. *Nature*, **438**, 842–845, doi: 10.1038/nature04313 (2005).

42. Piromallo, C., Becker, T.W., Funiciello, F., & Faccenna, C., Three-dimensional instantaneous mantle flow induced by subduction: *Geophys. Res. Lett.*, **33**, L08304, doi: 10.1029/2005GL025390 (2006).

43. Lowry, A. R., Ribe, N. M., Smith, R.B., Dynamic elevation of the Cordillera, western United States, J. Geophys. Res., **105**(B10), 23,371–23,390 (2000).

44. Sun, D., Chu, R., Helmberger, D., Refining tomographic images beneath Yellowstone by Waveform modeling; Part 2,Upper-Mantle, EarthScope National Meeting abstract (2009).

45. Waite, G. P., R. B. Smith, and R. M. Allen (2006), VP and VS structure of the Yellowstone hot spot from teleseismic tomography: Evidence for an upper mantle plume, J. Geophys. Res., 111, B04303, doi:10.1029/2005JB003867.

46. Anders, M. H. & Sleep, N. H., Lithospheric strengthening by magmatic intrusion: Thermal and mechanical effects of the Yellowstone hotspot, *J. Geophys. Res*., **97**, 15, 379-394 (1992).

47. Lithgow-Bertelloni, C. & Richards, M. A. The dynamics of Cenozoic and Mesozoic plate motions. *Rev. Geophys.,* **36**, 27–78 (1998).

48. Coney, P. J., in *Cordillerian metamorphic core complexes* (eds Crittendon, M. D., Coney, P. J., & Davis, G. H.), Geol. Soc. Am. Memoir **153**, 7–31 (1980).

49. Humphreys, E. D., et al., How Laramide-age hydration of North American lithosphere by the Farallon slab controlled subsequent activity in the western U. S., *Int. Geol. Rev*., **45**, 575–595 (2003).

Figure 1. Reference maps. a) P-wave (V_P) anomaly at 90 km depth, overlain by map of western U.S. tectono-magmatic domains. The plate margin and the Basin and Range, including the Rio Grande Rift (RGR) eastern Snake River Plain and Yellowstone (SRP-Y), are generally slow, though punctuated by high-velocity features. The Colorado Plateau is relatively fast with slow margins, especially beneath the west and south. Basin and Range is shown with red-on-white line, and the eastern extent of the tectonically disrupted western U.S., the Rocky Mountain Front, is shown with red and white dotted line. b) The ~2500 stations used for P-wave dataset: EarthScope Transportable Array (red triangles) and Flex Arrays (blue squares), and permanent networks and legacy temporary arrays (black dots).

Figure 2. Selected maps of V_P and V_P/V_S . a) V_P/V_S at 90 km depth. Selected zones of inferred partially molten, upwelling asthenosphere shown (from south to north: Salton Trough, edge of Gorda slab and Clear Lake volcanic field, SRP-Y hotspot track from 11 Ma caldera to active Yellowstone caldera). Partially molten asthenosphere also is inferred below the Colorado Plateau margins, especially to the west. b) V_P at 125 km depth. Cross section D-D' (across Yellowstone) is

shown in Fig. 4. c) V_P at 195 km depth with prominent fast anomalies shown (from west to east: Juan de Fuca-Gorda slab, southern Sierra drip, Wallowa drip, Siletzia curtain, Colorado Plateau drips, inferred basally accreted ocean plateau lithosphere). d) V_P at 270 km depth. Cross sections are shown in Fig. 3.

Figure 3. Cross-sections extending from 60–800 km depth with 410 km and 670 km discontinuities (black-dashed). a) Latitude 41° V_P cross-section (A-A', Fig. 2d), showing fast Juan de Fuca-Gorda slab, slow Great Basin, fast slab in the transition zone (probably subducted ~30-55 Ma), and fast fragment of basally accreted plateau lithosphere (accreted ~60 Ma). b) V_P cross section (B-B', Fig. 2d) showing high velocity body inferred to be melt depleted ocean plateau lithosphere. c) V_P cross section (C-C', Fig. 2d) showing fast Wallowa drip (left) and Siletzia curtain (right).

Figure 4. Yellowstone cross-section D-D' (Fig. 2b), extending from 60–800 km depth with 410 km and 670 km discontinuities (black-dashed). All panels show the same section. Images from (left) isolated V_P and (center) V_S inversions, and (right) jointly inverted V_P/V_S model. Note range of velocity scale increased to enhance details of strongly anomalous structure. Maximum velocity reduction in the section is 5.5% V_P, 12% V_S, and maximum V_P/V_S increase is 6%. The V_S inversion appears to connect the near-surface and transition zone low-velocity features. Elevated V_P/V_S in the upper ~180 km indicates partially molten mantle. The transition zone beneath Yellowstone also may be partially molten or exceptionally hydrated.

Supplementary Information

Data

Travel-time data come from 2500 temporary and permanent stations deployed in the western United States, southern Canada, and northern Mexico since 1986. Table 1 lists the networks used for P- and S-waves. Data from legacy temporary experiments and permanent broadband and short-period networks significantly improve our sampling of the upper mantle beyond that available with the Transportable Array (TA) alone.

We use direct P and PKPdf phases observed on the vertical component for measurement of P-wave residuals. S-wave data are rotated to radial and tangential components and residuals are measured from direct S phases observed on the tangential component. Residual times are measured by cross-correlation of band-pass-filtered waveforms in up to four narrow Gaussian frequency bands with center frequencies of 1 Hz, 0.5 Hz, 0.3 Hz, and 0.1 Hz for P-waves and 0.4 Hz, 0.1 Hz, and 0.05 Hz for S-waves. Data from short-period stations are only used for 1 Hz P-wave residuals times, and are also measured by cross-correlation. The r.m.s of P and S residuals is 0.42 s and 1.13 s, respectively.

Recent advances in western U.S. crust thickness and velocity models are used to calculate explicit corrections to travel-time residuals used in our mantle tomography. To correct for crust thickness variations we use a western U.S. Moho model created by a joint inversion of receiver functions, gravity, and heat flow[1]. For most of the western U.S., only mid- to upper-crust velocity variations (<12 km) are used in our corrections. The shallow S-velocity structure is taken from 8 s period ambient noise phase velocities[2], and we use a constant V_P/V_S of 1.78 to create a P-velocity model. We acknowledge the shortcomings of uniformly scaling V_S to V_P, but the potential errors introduced by a constant V_P/V_S

ratio are small compared to the errors that would be introduced by ignoring strong upper crustal structures such as basins and crystalline mountain ranges. In California[3,4] and near Yellowstone[5], higher resolution crust thickness and velocity models are used to calculate correction times. The r.m.s of crust correction times is 0.13 s and 0.26 s for P and S, respectively.

Methods

We use frequency-dependent 3-D sensitivity kernels to relate travel-time residuals to perturbations of model parameters. Several approximations are used in constructing these kernels. First, we use the single-scattering, "banana-doughnut," formulation of Dahlen et al.[6] We then apply smoothing normal to the ray path to address ray location uncertainty. The smoothing width increases with distance along the ray path in accord with ray location uncertainty, which we estimate based on the results of Saltzer and Humphreys[7]. For a 60º teleseism, the smoothing width increases from 2 km to 15 km between the Moho and the base of the transition zone. Finally, the smoothed kernels are approximated by a function that depends on the dominant period of the waveform, epicentral distance, distance normal to the geometric ray, distance along the geometric ray, and ray-centered azimuth. These computationally efficient approximations are appropriate because any intricate structure of the kernels, for the periods used in our study, will be aliased when the sensitivity values are integrated onto discrete model parameters with a mean spacing of ~45 km. The main benefit of 3-D sensitivity kernels is that they provide an approximate means to interpret frequency dependence of travel-time residuals, thus allowing better use of broadband data and imposing physically based smoothness criteria on the inversion. For short-period data, we use geometrical ray theory to calculate partial derivatives because the data are band-limited and 1 Hz first-Fresnel zone radii are generally smaller than or similar to the node spacing.

Nodes at the vertices of an irregular 3-D mesh parameterize the model space (Fig S1). Node spacing increases progressively from 30 km to 60 km with depth to address decreasing resolution. Horizontal node spacing is smallest beneath the array footprint and gradually increases moving outward to address the paucity of crossing-ray coverage in deeper volumes near and outside the array footprint. Horizontal node spacing varies from 38 to 60 km. The model space extends from 36 (top of AK135 mantle) to 850 km depth and laterally it extends 800 km beyond the farthest station in every direction.

In addition to the V_P and V_S model parameters, we invert for station and event parameters. Because we correct for crust thickness and velocity variations, the station terms are only intended to address local site effects and errors in the crust model; consequently, we apply strong station damping to keep the station terms from absorbing mantle structure. The r.m.s. of the station terms is 0.06 s and 0.1 s for P and S, respectively. Event terms represent adjustment of the mean arrival time for the specific set of stations that record each event. These terms are important because we solve for velocity perturbations rather than absolute velocity, and the mean velocity structure varies significantly for different sub-arrays in the provincially heterogeneous western U.S. For example, the inversion finds that P arrivals to Nevada are ~0.35 seconds later than arrivals to eastern Montana when averaged over all azimuths and ray parameters. Because of the migration of the TA, Nevada and eastern Montana sub-arrays do not share common events, but the overlapping patchwork of sub-arrays allows the inversion to find the difference in mean structure that is optimal with respect to the entire western U.S. dataset.

Gradient damping and norm damping are used to regularize the inverse problem. The geometry of the gradient damping is asymmetric such that the weight of the constraint is greatest in the plane normal to the mean ray path orientation as a function of depth. In the uppermost mantle, where teleseismic ray paths are nearly vertical, horizontal gradient damping receives 2.5x the weight of vertical gradient damping. The relative horizontal/vertical weight decreases smoothly with depth to account for the increasing angle of inclination of teleseismic ray paths away from the receiver. At the base of the transition zone, 670 km, the horizontal/vertical ratio is ~1.5. Norm damping seeks to find the smallest model that satisfies the travel-time data. Given the abundance and diversity of ray paths sampling the western U.S. upper mantle we prefer to keep norm damping small so as to more accurately recover the amplitude of anomalous structures.

We find an optimal solution to the regularized inverse problem by using the LSQR method[8] to minimize the cost function

$$E = ||A\mathbf{m} - \mathbf{d}||^2 + k_1||L\mathbf{m}||^2 + k_2||\mathbf{m}||^2.$$

Vector **m** contains the model parameters, and matrix A contains the partial derivatives that relate travel-time residuals to perturbations in model parameters; **d** is the data after crust corrections. The relative weights of the damping terms are given by k_1 and k_2. The L matrix represents the spatially varying smoothing constraint described above. We do this individually for the V_P and V_S models.

We also construct a joint V_P and V_S model, which is found by simply summing the individual cost functions and adding additional regularization for V_P/V_S values.

$$E_{Vp/Vs} = E_{Vp} + E_{Vs} + k_3||L_{Vp/Vs}\mathbf{m}||^2$$

Damping the gradient of V_P/V_S variations regularizes the V_P/V_S model. Thus, we allow for significant departures from the reference V_P/V_S values of AK135, but we simultaneously impose smoothness constraints on P, S, and V_P/V_S structure. The P and S datasets are equally weighted in the joint inversion.

Synthetic tests demonstrate expected model resolution with the assumption of an isotropic, elastic mantle. The synthetic structure consists of several checkerboard layers embedded in a neutral background. In general, the recovery of the input structure is excellent, but there is some streaking and amplitude decay of the input structures owing to the sub-vertical orientation of teleseismic rays, regularization, and preference for minimum energy structure in the inversion algorithm. Fig. S2

Results

The tomographic models presented in this paper achieve the following variance reductions with respect to the measured travel-time residuals:

Isolated P inversion - 88.3%

Isolated S inversion - 85.8%

Coupled P and S inversion

Total - 82.1%

P - 80.7%

S - 83.6%

Interpretation of V_P/V_S structure

With teleseismic data, V_P/V_S anomalies can be caused by lateral variations in radial anisotropy, rock composition, or partial melt. Because the volumes of highest V_P/V_S underlie areas of young magmatism, the presence of partially molten mantle obviously has an important influence. Expected radial anisotropy created by upper mantle flow would have ascending and flattening low-velocity volumes and vertically lengthening high-velocity volumes, which would create the opposite effect on V_P/V_S than what is observed for low-velocity anomalies. Potential compositional influences on mantle

V_P/V_S include hydration, whose effects are relatively modest in the shallow upper mantle[9], and melt depletion. Hydration of the western North America lithosphere[10] and asthenophere[11] has been suggested. In general, the possibility of asthenospheric hydration[11,12], is regionally supported by the occurrence of strongly depressed velocities beneath western U.S. to depths of 150 - 200 km[14,15], but hydration alone cannot account for 4% peak-to-peak V_P/V_S variations in the same depth range[9]. Melting deeper than ~70 km necessitates elevated mantle temperatures or the presence of dissolved volatiles. Away from the Yellowstone area[16] there is no evidence for greatly elevated asthenosphere temperatures, leading us to conclude that a small amount of dissolved volatile enables deep asthenospheric melting. There is not consensus as to how strongly melt depletion affects V_P/V_S[17,18]. Melt depletion is generally thought to lower V_P/V_S at least slightly, but alone it is unlikely to account for the magnitude of variations we find in the western U.S. Hence, we think that the slowest volumes of mantle, which have very high V_P/V_S, are partially molten. Regional teleseismic tomography does not constrain absolute V_P or V_S value, consequently absolute V_P/V_S is not constrained. However, the 4% peak-to-peak V_P/V_S variation that is commonly imaged to depths of ~160 km is consistent with subsolidus fast mantle and ~1% melt fraction in the slow mantle[19]. Further supporting the idea that the low-velocity upper mantle is partially molten is the observation that the slowest mantle tends to underlie areas thought to have very thin lithosphere (i.e., most of California and the Basin and Range).

Table 1.

Data Source	P	S	Info
TA	X	X	temporary broadband (BB)
US	X	X	permanent BB
SCSN	X	X*	sCA permanent, BB and short-period (SP)
NCSN	X	X*	nCA permanent, BB and SP
PNSN	X	X*	WA and OR permanent, BB and SP
Yelowstone SP	X		permanent SP
U. Utah	X	X*	permanent BB and SP
Montana	X		permanent SP

Intermountain West	X	X	permanent BB
Mendocino FA	X	X	temporary BB
Wallowa FA	X	X	temporary BB
High Lava Plains FA	X	X	temporary BB
SNEP FA	X	X	temporary BB
CAFE FA	X	X	temporary BB
SIEDCAR FA	X	X	temporary BB
OATS	X	X	temporary BB
La RISTRA	X	X	temporary BB
CDROM	X	X	temporary BB
Billings	X	X	temporary BB
Yellowstone 1999-00	X	X	temporary BB
LARSE II 1998	X		Los Angeles – Mojave, temporary BB and SP
SPE 1997	X	X	Southern Sierras, temporary BB
Deep Probe**	X		temporary BB and SP
RGR 1995**	X		temporary BB
SRP 1993	X	X	temporary BB
S. Oregon 1986**	X		temporary SP
NTS**	X		temporary SP, Nevada Test Site

*S data only from BB stations
**used archived residual times from Humphreys et al., 2003

1. Lowry, A. R., Squeezing Mass Structure from EarthScope TA Data, EarthScope National Meeting abstract, (2009).

2. Lin, F-C., Moschettie, M. P., Ritzwoller, M. H., Surface wave tomography of the western United States from ambient seismic noise: Rayleigh and Love wave phase velocity maps,

Geophys. J. Int. **173**, 281–298 doi: 10.1111/j.1365-246X.2008.03720.x (2008).

3. Lin, G., P. M. Shearer, E. Hauksson, and C. H. Thurber (2007), A 3-D crustal seismic velocity model for Southern California from a composite event method, Journal of Geophysical Research.

4. Thurber, C., H. Zhang, T. Brocher, V. Langenheim, Regional three-dimensional seismic velocity model of the crust and uppermost mantle of northern California, J.

Geophys. Res., **114**, B01304, doi:10.1029/2008JB005766 (2009).

5. Stachnik, J. C., Dueker, K., Schutt, D. L., and Yuan, H., Imaging Yellowstone plume-lithosphere interactions from inversion of ballistic and diffusive Rayleigh wave dispersion and crustal thickness data, Geochem. Geophys. Geosyst., **9**, Q06004, doi:10.1029/2008GC001992 (2008).

6. Dahlen, F.A., Hung, S.-H., Nolet, G. (2000) Frechet kernels for finite-frequency traveltimes, I. Theory, *Geophys. J. Int*., **141**, 157–174 (2000).

7. Saltzer, R. L., & Humphreys, E. D., Upper mantle P wave velocity structure of the eastern Snake River Plain and its relationship to geodynamic models of the region, *J. Geophys. Res.*, **102**, 11,829 – 11,841 (1997).

8. Paige, C. C., & Saunders, M. A., LSQR: An algorithm for sparse linear equations and sparse least squares, *ACM Trans. Math. Soft*., **8**, 43–71 (1982).

9. Jacobsen, S. D., et al., Effects of hydration on the elastic properties of olivine, *Geophys. Res. Lett.*, **35**, L14303 (2008).

10. Humphreys, E. D., et al., How Laramide-age hydration of North American lithosphere by the Farallon slab controlled subsequent activity in the western U. S., *Int. Geol. Rev*., **45**, 575–595 (2003).

11. Yang, Y., Forsyth, D. W., Attenuation in the upper mantle beneath Southern California: Physical state of the lithosphere and asthenosphere, *J. Geophys. Res*., **113**, B03308, doi:10.1029/2007JB005118 (2008).

12. Karato S., Jung H., Water, partial melting and the origin of seismic low velocity and high attenuation zone in the upper mantle. *Earth Planet Sci Lett*., **57**, 193-207 (1998).

13. Dixon, J.E., T.H. Dixon, D.R. Bell, R. Malservisi, Lateral variation in upper mantle viscosity: role of water, *Earth Planet. Sci. Lett.,* **222**, 451–467 (2004).

14. Lebedev, S. & van der Hilst, R., Global upper mantle tomography with the automated inversion of surface and S-waveforms, Geophys. J. Int., **173**, 505-518 doi: 10.1111/j.1365-246X.2008.03721.x (2008).

15. Bedle, H., & van der Lee, S., S velocity variations beneath North America, *J. Geophys. Res.*, **114**, B07308, doi:10.1029/2008JB005949 (2009).

16. Schutt, D. L., Dueker, K., Temperature of the plume layer beneath the Yellowstone hotspot, *Geology*, **36**, no. 8, 623–626, doi: 10.1130/G24809A (2008).

17. Lee, C.-T. A., Compositional variation of density and seismic velocities in natural peridotites at STP conditions: Implications for seismic imaging of compositional heterogeneities in the upper mantle, *J. Geophys. Res.*, **108**(B9), 2441, doi:10.1029/2003JB002413, (2003).

18. Schutt, D. L. & Lesher, C. E., Effects of melt depletion on the density and seismic velocity of garnet and spinel lherzolite, *J. Geophys. Res.*, **111**, B05401, doi:10.1029/2003JB002950 (2006).

19. Hammond, W. C., & E. D. Humphreys, Upper mantle seismic wave velocity: Effects of realistic partial melt geometries, *J. Geophys. Res.*, **105** (B5),975–986 (2000).

Supplementary figure captions:

Fig. S1. Parameterization of the western U.S. mantle. One constant depth shell of nodes (blue dots) is displayed, horizontal node spacing does not vary with depth.

Fig. S2. P-wave resolution test. The input, synthetic structure, consists of 3 checkerboard layers separated by neutral layers in order to show how well anomalous structure is recovered as well as the potential for streaking anomalous structure into neutral domains. The peak magnitude of structures in the inverted model is typically 75% of the peak magnitude of the input structure (+/- 3%). Resolution decays near the eastern margin because the TA recently occupied this area.

Fig. S3. P-velocity maps.

Fig. S4. S-velocity maps.

Fig. S5. V_P/V_S maps.

Fig. S6. Joint P- and S-velocity maps.

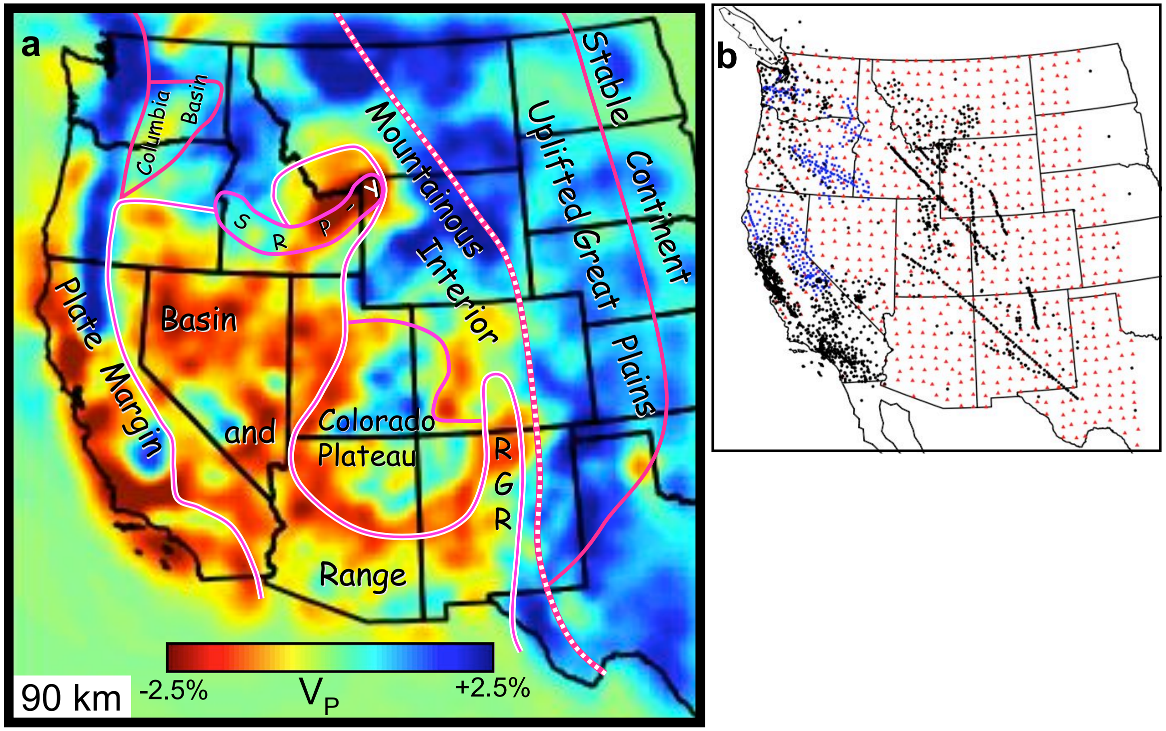
a
b
Columbia
Basin
Mountainous
Interior
Stable
Continent
Uplifted Great
Plains
S
R
P
Y
Plate
Margin
Basin
and
Range
Colorado
Plateau
R
G
R
90 km
-2.5%
V_P
+2.5%

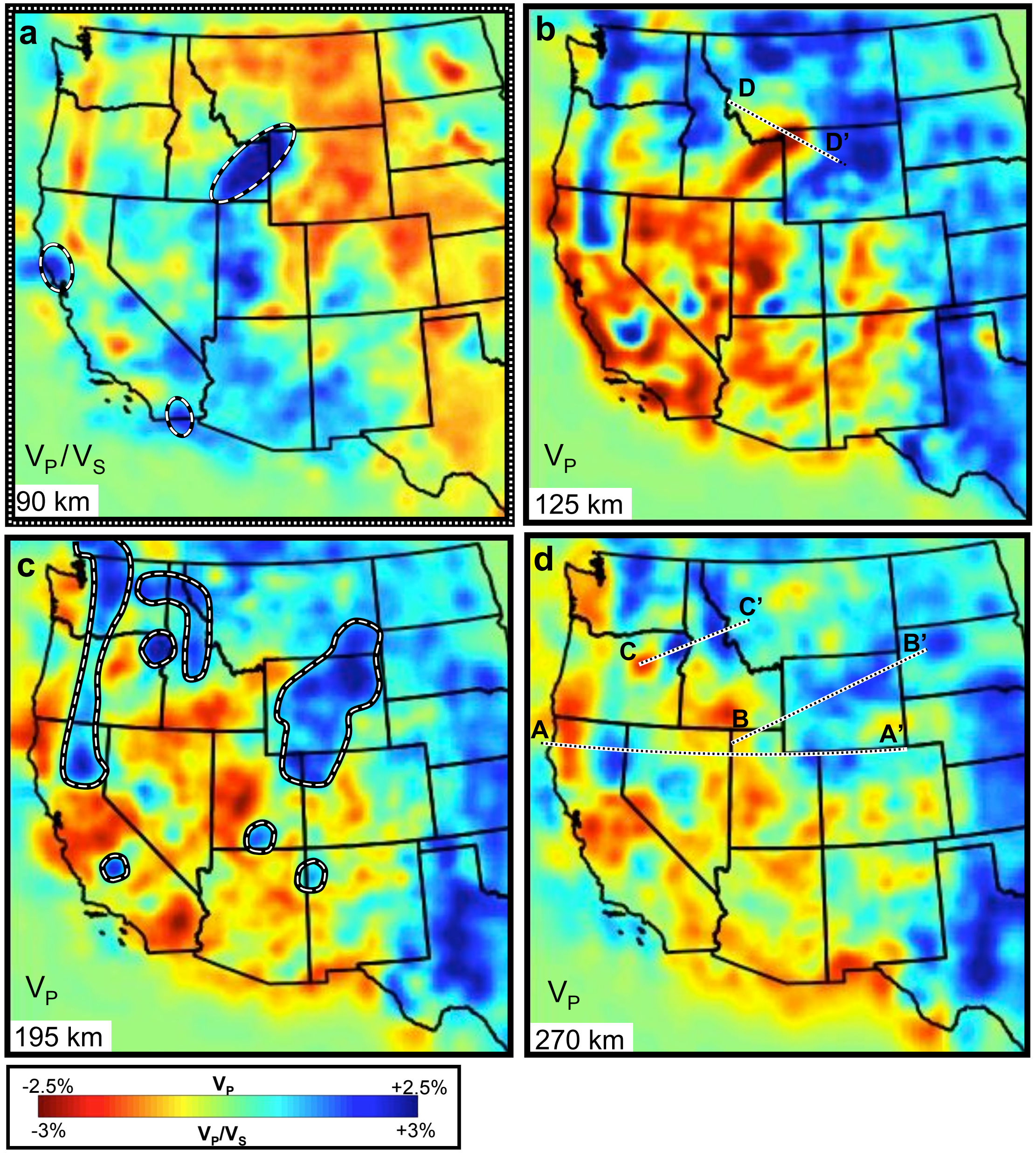

a
VP/VS
90 km
b
D
D'
VP
125 km
c
VP
195 km
d
C'
C
B'
B
A
A'
VP
270 km
-2.5%
VP
+2.5%
-3%
VP/VS
+3%

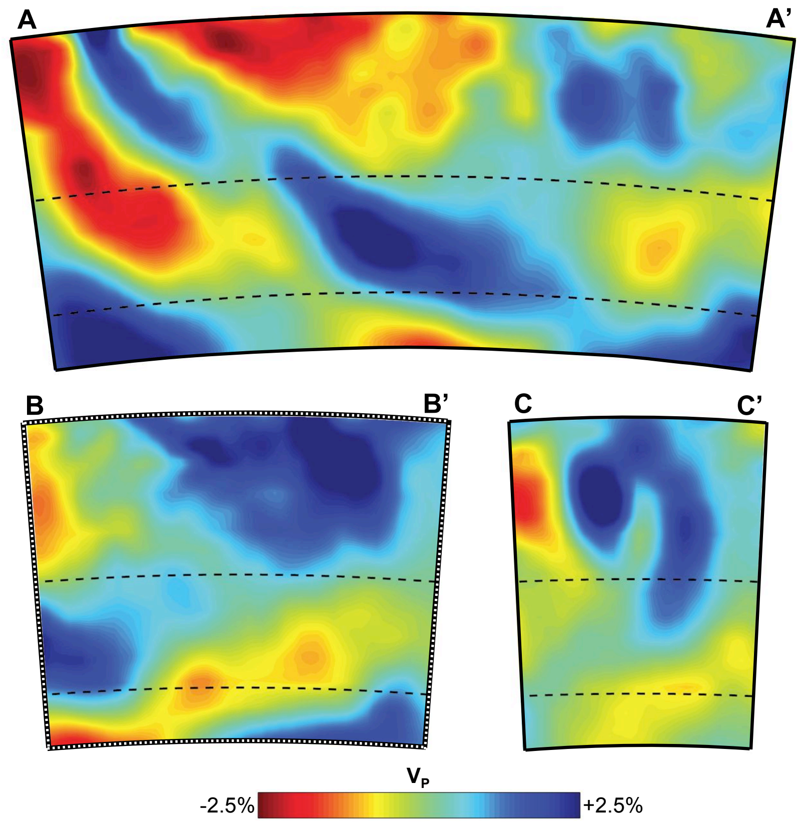
A
A’
B
B’
C
C’
V
-2.5%
+2.5%

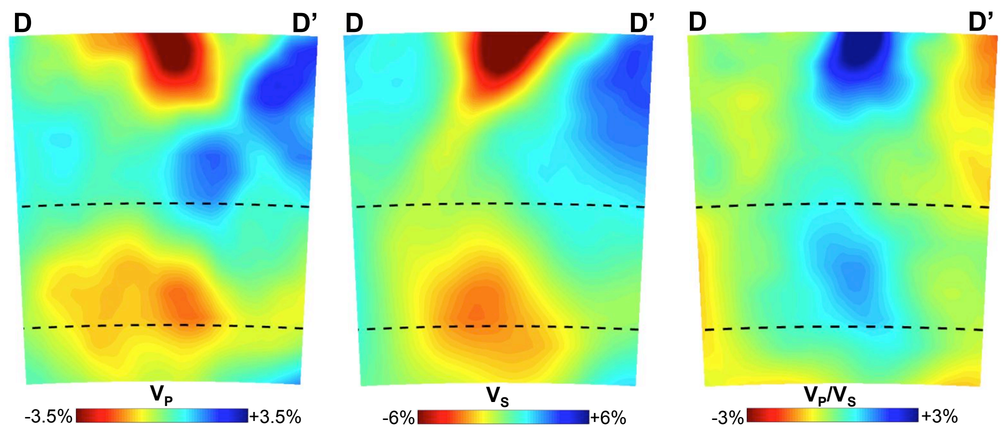
D
D’
D
D’
D
D’
V_P
-3.5%
+3.5%
V_S
-6%
+6%
V_P/V_S
-3%
+3%

Fig. S1

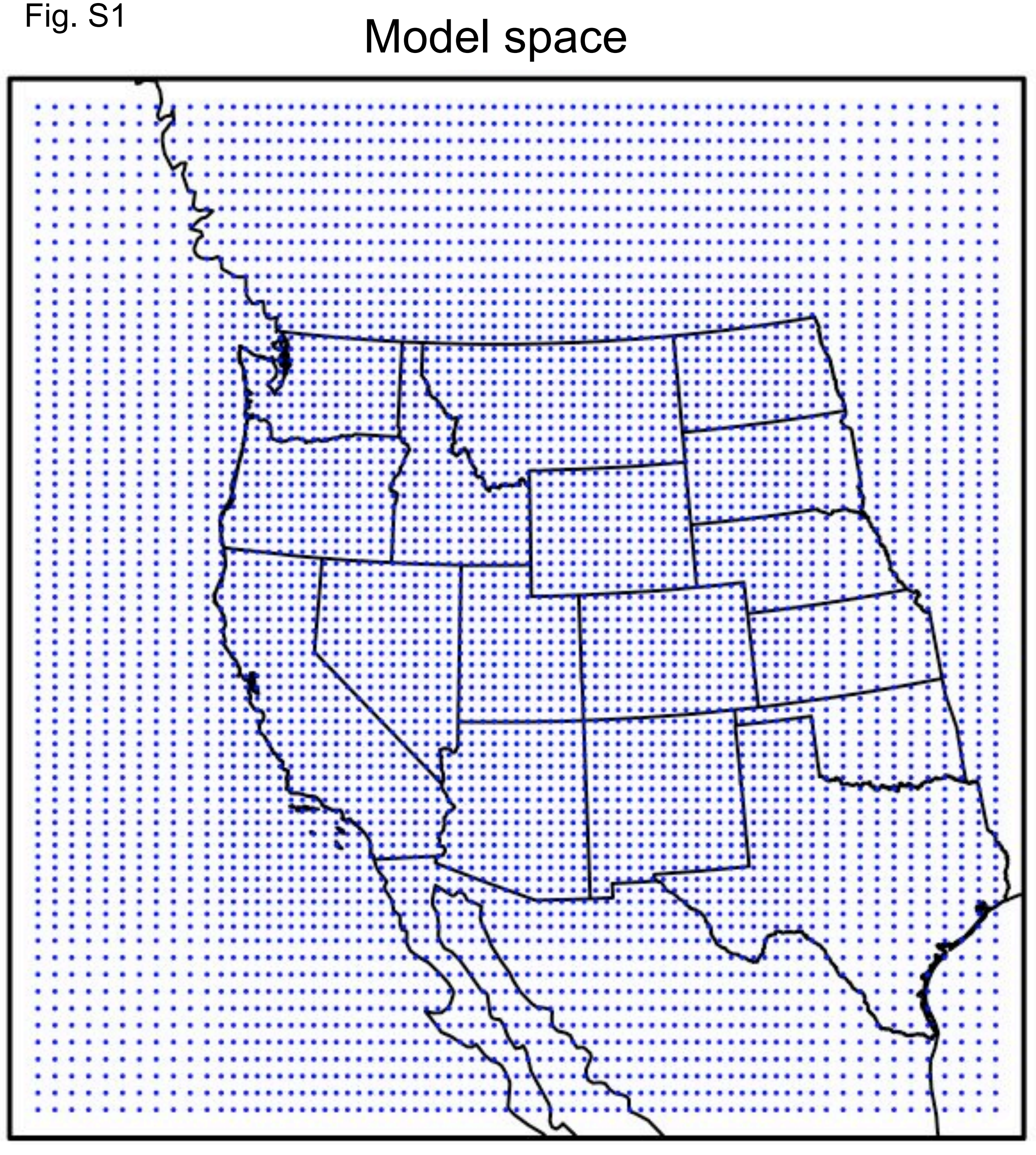

Fig. S2 P-wave synthetic test

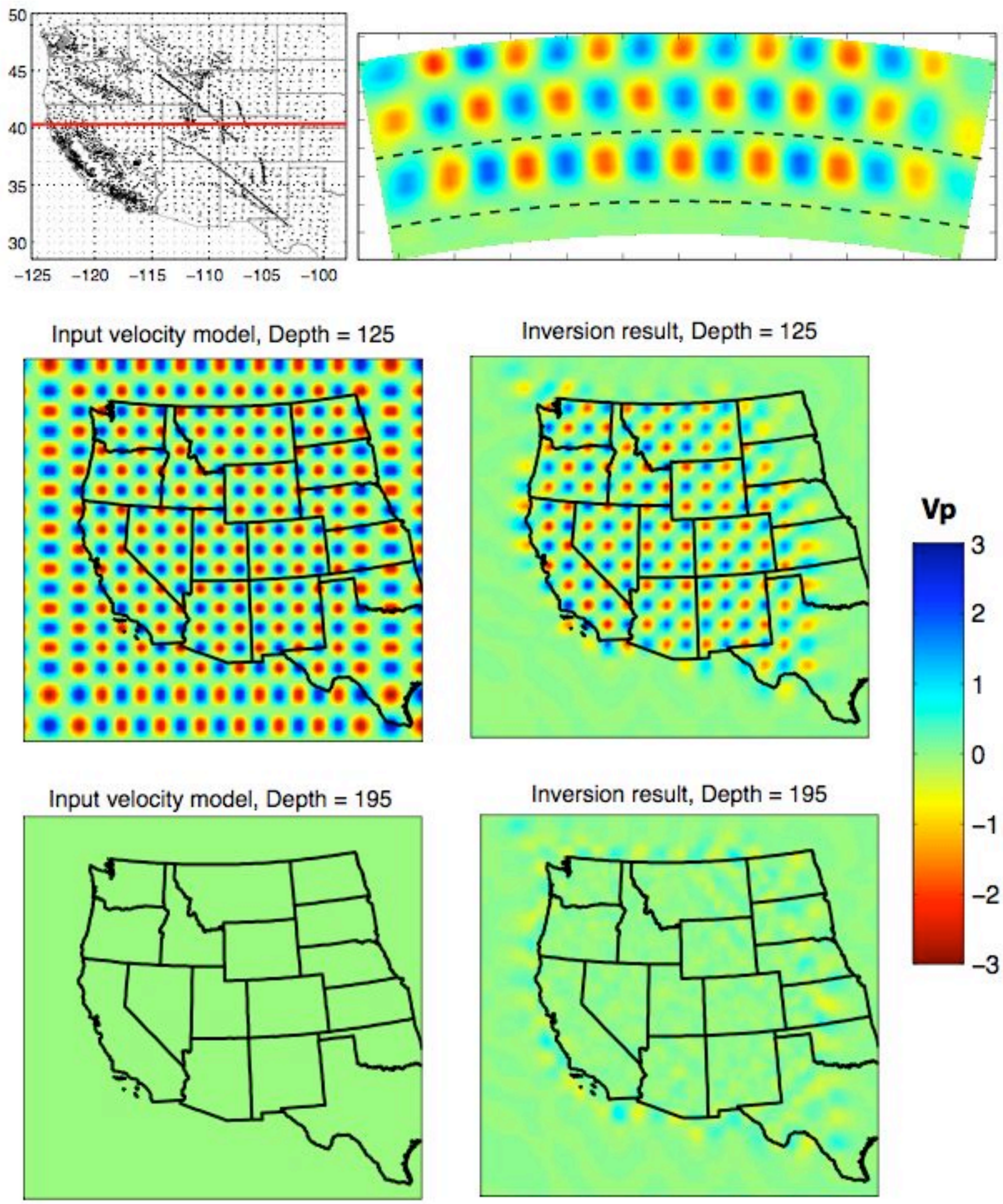

Fig. S3

P-velocity maps

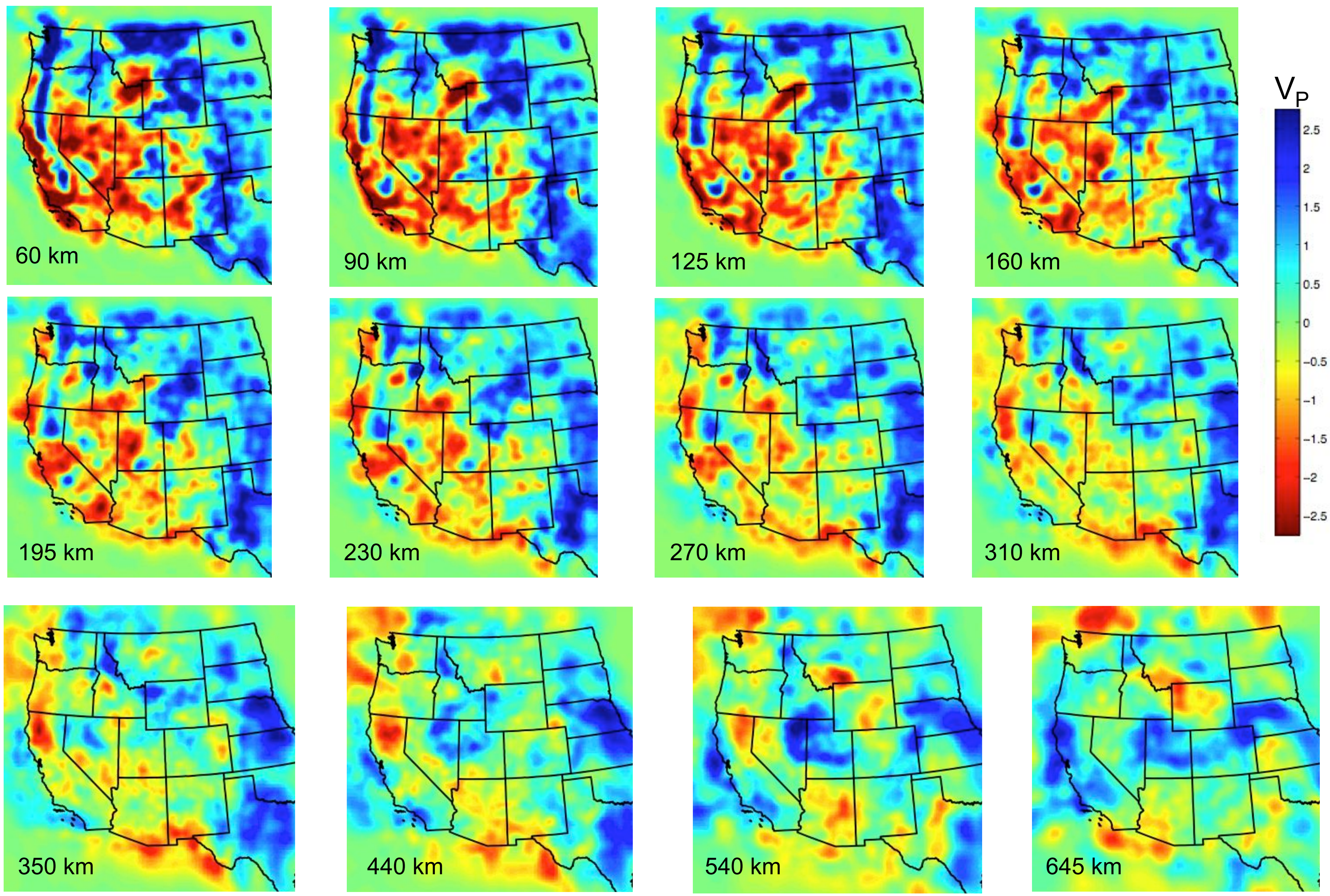

Fig. S4

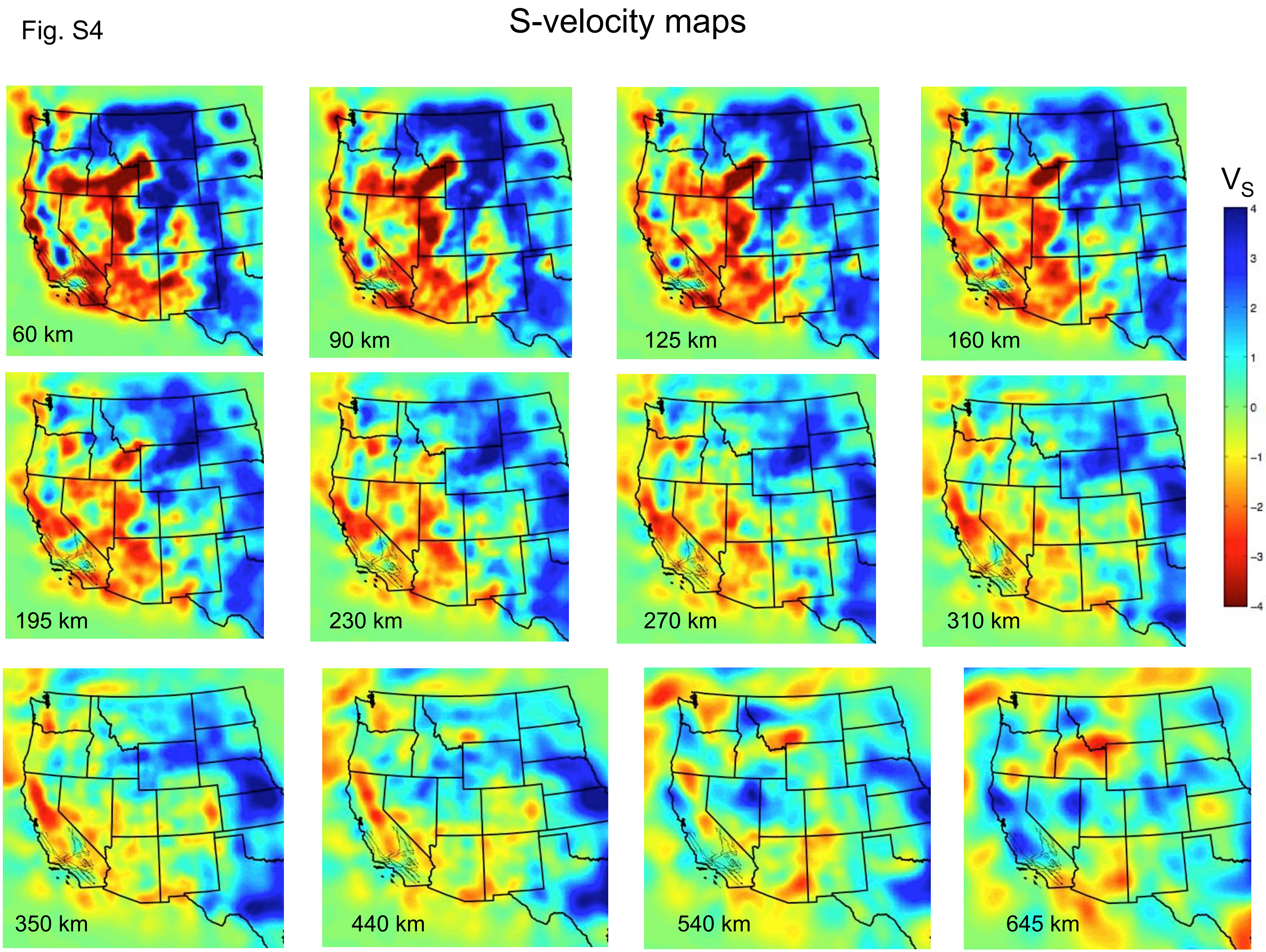
S-velocity maps
60 km
90 km
125 km
160 km
195 km
230 km
270 km
310 km
350 km
440 km
540 km
645 km
V_S
4
3
2
1
0
−1
−2
−3
−4

Fig. S5

V_P/V_S maps

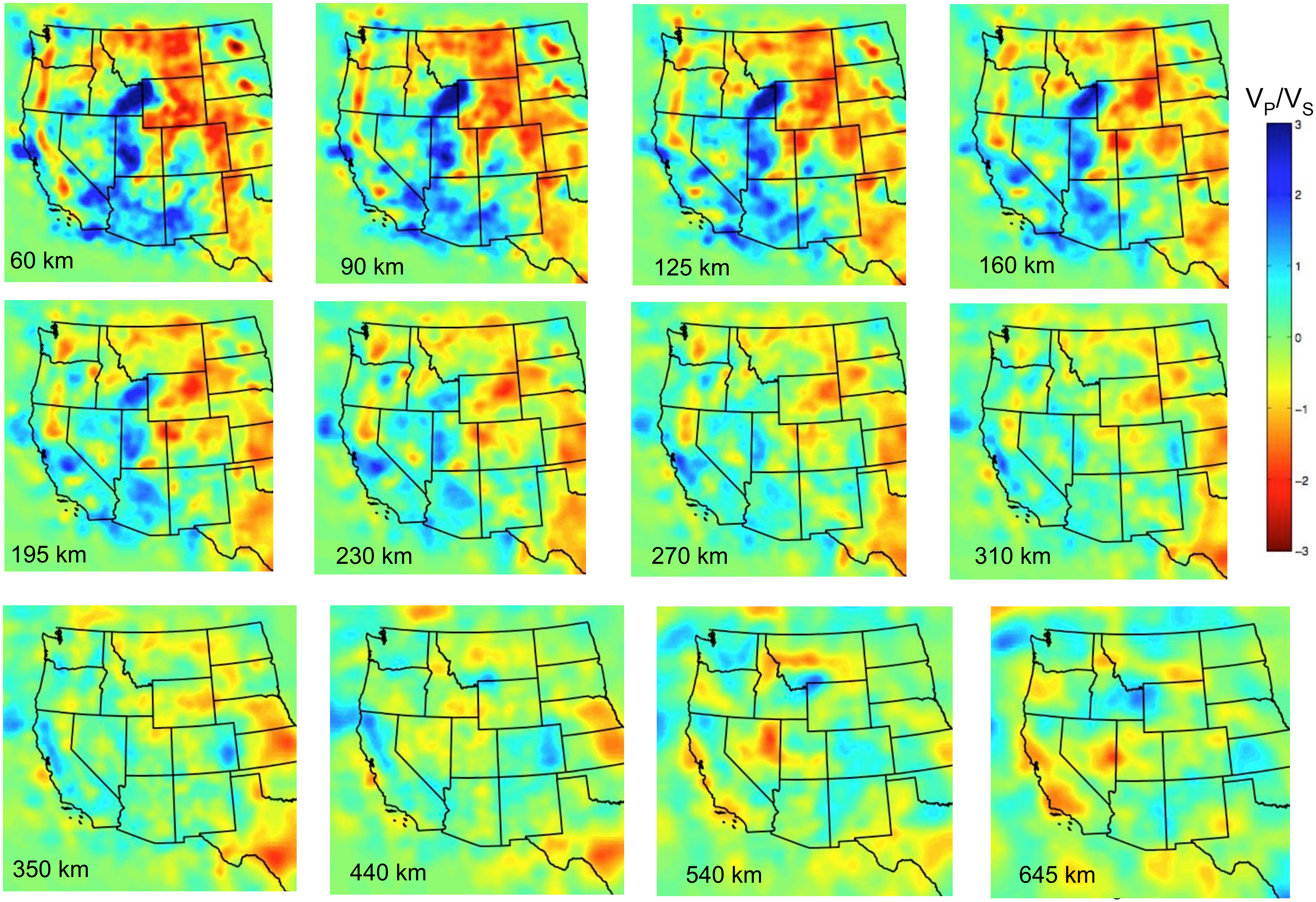

Fig. S6 V_P and V_S maps from joint inversion

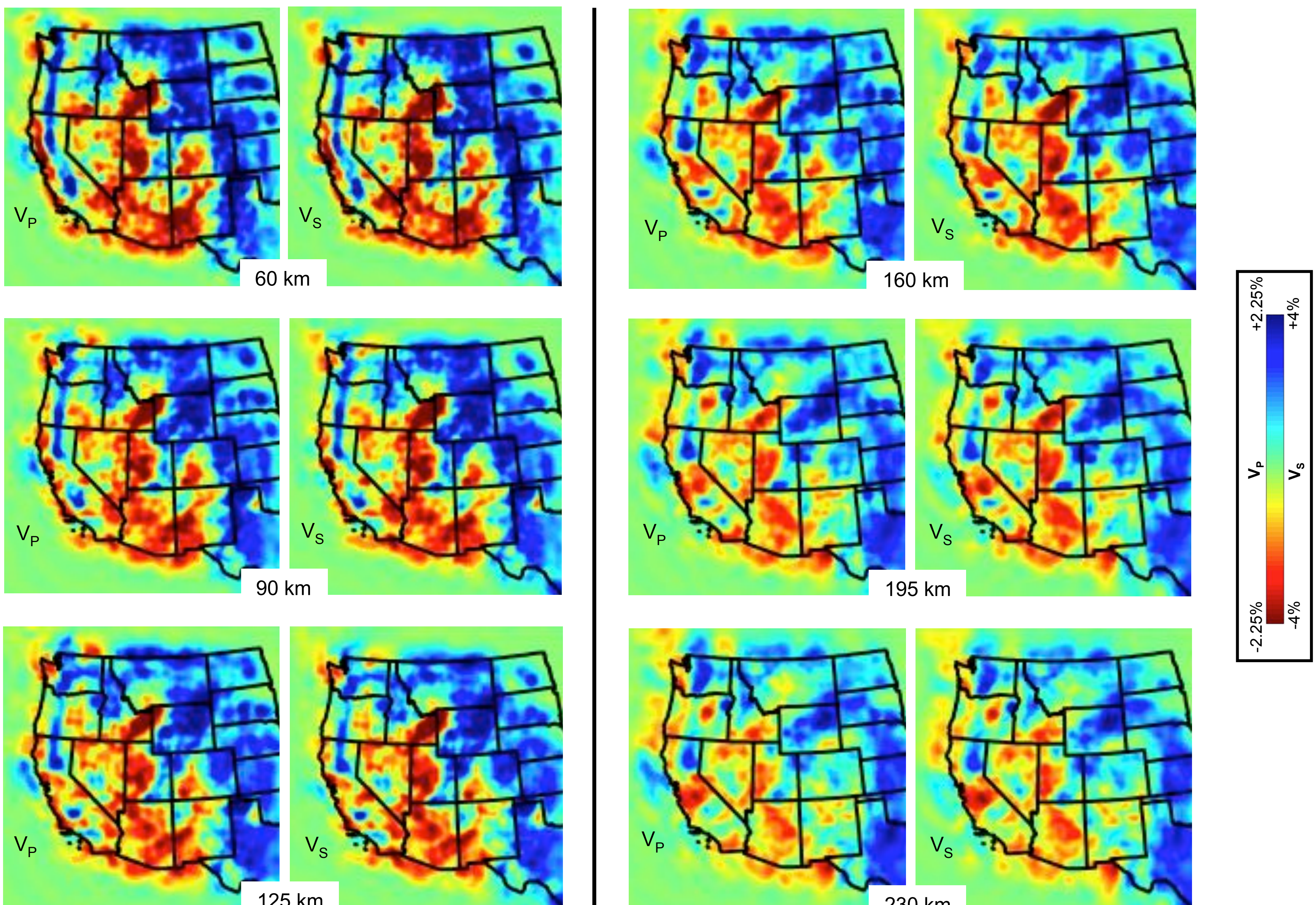

Fig. S6

V_P and V_S maps from joint inversion